Japan Architectural Review
Open Access
Architectural Institute of Japan

Translated Paper

Superior design solutions of section sizes in steel buildings for different lateral frame systems and column shapes

Jiro Takagi[1] Ruka Obana[2] and Makoto Ohsaki[3]

[1]Graduate School of Urban Environmental Sciences, Tokyo Metropolitan University, Hachioji-shi, Tokyo, Japan; [2]Department of Architecture and Architectural Engineering, Tokyo Metropolitan University, Hachioji-shi, Tokyo, Japan; [3]Department of Architecture and Architectural Engineering, Kyoto University, Kyoto, Japan

Correspondence
Jiro Takagi, Graduate School of Urban Environmental Sciences, Tokyo Metropolitan University, 1-1 Minamio-sawa Hachioji-shi, Tokyo 192-0397, Japan.
Email: jtakagi@tmu.ac.jp

Funding Information
JSPS KAKENHI.

The Japanese version of this paper was published in Volume 84 Number 763, pages 1293-1303, https://doi.org/10.3130/aijs.84.1293 of *Journal of Structure and Construction Engineering (Transactions AIJ)*. The authors have obtained permission for secondary publication of the English version in another journal from the Editor of *Journal of Structure and Construction Engineering (Transactions AIJ)*. This paper is based on the translation of the Japanese version with some slight modifications.

Received January 9, 2020; Accepted April 1, 2020

doi: 10.1002/2475-8876.12156

Abstract

Superior design solutions of 7-story steel buildings are obtained by the multiple start local search (MSLS) method, minimizing the steel volume for three types of structural systems: a space-frame system with rectangular hollow structural section (HSS) columns (SFS), perimeter-frame system (PFS) with I-shaped columns (PFSH), and a PFS with rectangular HSS columns (PFSB). Most beam-to-column connections are moment connections in SFS, whereas they are limited in PFS. In terms of steel volume, PFSH is advantageous for moment-frame buildings, and SFS and PFSB are suitable for braced frames with uniform column spacings. SFS is disadvantageous for mixed-, moment-, and braced-frame buildings.

Keywords
lateral frame location, multiple start local search, response history analysis, steel structure, ultimate lateral strength

1. Introduction

Beam-to-column connections of steel buildings consist of two types: moment connections and pinned connections. The flanges of beams are rigidly connected to columns in the moment connections, whereas they are not in pinned connections. The lateral frames are composed of columns and beams with moment connections, and the gravity frames are composed of those with pinned connections. Steel buildings in Japan mostly have lateral frames, whereas in other countries including the United States, lateral frames are limitedly placed typically in perimeter frames separately from gravity frames. In this paper, the former system is referred to as the space-frame system (SFS) and the latter as the perimeter-frame system (PFS). Rectangular hollow structural section (HSS) columns are normally used in SFS, and I-shaped columns are used in PFS. Past research[1–6] has focused on the differences of these systems; however, the buildings compared may not be evenly and rationally designed and discussion on the findings of their structural characteristics may not always be objective.

The authors proposed an algorithm to obtain superior design solutions for SFS and PFS for 7-story office buildings and compared their structural characteristics.[7,8] The multiple start local search (MSLS) approach was used to obtain superior solutions, minimizing the steel volume with discrete variables of the section sizes. The solutions satisfy many structural design requirements in the building codes of allowable stress design and ultimate lateral strength. The superior solutions of SFS and PFS systems obtained through this algorithm are independent of designers' skills or experiences. Their structural characteristics were objectively discussed, and dominant design requirements or constraints were identified. A comparison revealed that the steel volume of PFS is smaller than that of SFS. Additionally, the steel volumes of the superior solutions are smaller than the statistical average of the steel buildings in the same sizes. This fact confirms the effectiveness of MSLS. Furthermore, the solutions do not satisfy the Japanese design requirements for very rare (L2) earthquakes evaluated by response history analyses, indicating inconsistencies between structural design methods.

In this study, superior design solutions with different structural systems and building structures are designed to satisfy many structural design requirements including the ultimate lateral strength defined in response history analyses for L2 earthquake records. Structural characteristics and responses for the L2 response history analyses are examined from various aspects. A previous study[8] by the authors is extended and the properties of a new structural system, PFSB (where rectangular HSS columns are used in a PFS), are evaluated. The traditional PFS using I-shaped columns is re-defined as PFSH for comparison with PFSB. SFS, PFSH, and PFSB are examined for moment-frame and braced-frame buildings. Round HSSs and buckling restrained braces (BRB) are examined for the braced frames. Furthermore, mixed-frame structures with moment and braced frames are investigated. The effects of lateral frame locations and column shapes on the steel volume are evaluated. The possibility of a new structural design approach is suggested.

It should be noted that "braced-frame structure" in this paper means dual moment frame with concentrated braces defined in ASCE,[9] and not pinned gravity frame with concentrated braces. Similarly, "BRB structure" means dual moment frame with concentrated BRB braces. Furthermore, "mixed-frame structure" means moment frame in one direction and above-described braced frame in the orthogonal direction.

2. Outline of Building Examined and Structural Design Approach

2.1 Outline of building

A rectangular 7-story steel office building with 32.0 × 19.2 m plan is examined. The size of the building plan is the same as that examined in the previous work;[8] however, the column spacing is uniform at 6.4 m in this study. Moment-frame and braced-frame structures as shown in Figure 1 are investigated. The building is simplified in order to identify general structural characteristics. The solid triangles in Figure 1 indicate moment connections and the others represent pinned connections. All beam-to-column connections are moment connections and all frames are lateral frames in SFS, while four frames in the perimeters are the lateral frames and the others are the gravity frames in PFS.

Figure 2 shows the frame elevations for the braced frames with concentrated braces. The geometry is the same for the moment frames except for the existence of the braces. More braces are placed than general design. The flexural deformation of the multi-story braced frames is restrained, and shear deformation is dominant. Therefore, additional axial forces in the columns in the braced frames under seismic lateral loads do not have much effect on the column design. The solid triangles in the columns on second and fifth stories in Figure 2 indicate the splices. The segments between the column splices are called "parts" and the member sections are grouped in each part. The names of columns and beams are shown in Figures 1 and 2. GX2 and GY2 in the figures for PFS are pinned at the ends and designed only for the gravity load. However, these names are kept identical between the PFS and SFS for simplicity.

The grouped member sections are shown in Table 1. The columns are rectangular HSS or I-shaped sections, and the beams and braces are I-shaped sections and round HSSs, respectively. The steel grade is assumed to be SN490 and the design standard strength (almost nominal yield strength) is 325 N/mm^2.

2.2 Structural design approach

A two-step structural design approach is assumed for the structural design of the building; this is based on the allowable stress design for gravity and seismic design loads (first step) and ultimate lateral strength design for earthquakes (second step).[10] Elastic analysis and inelastic pushover analysis are performed in the first and second steps, respectively. More information about Japanese structural design procedure can be found in Michel Bruneau et al.[11] The composition of floor structure and calculated weight are summarized in Appendix 1. The vertical distribution factor A_i[12] is adopted. The vibration characteristic factor R_t and seismic zone factor Z[12] are both assumed to be 1.0. The seismic base-shear coefficient C_0 is 0.2 for the allowable seismic design. Two types of the required ultimate lateral strength are defined in the second seismic design step; these are based on the code-required strength taking into account the ductility of members (member ranks) and are defined in reference to responses in response history analyses for L2 earthquakes. For the code-required strength, the shape factor F_{es}[12] is assumed to be 1.0, and the required base-shear coefficient C_{QUN1} is 0.3 and 0.35 for moment-frame and braced-frame structures, respectively. These values are defined with the structural characteristic factor D_s with the ranks A or B of the composing members. However, C_{QUN1} is assigned as 0.6 for moment frames and 1.0 for braced frames, referring to

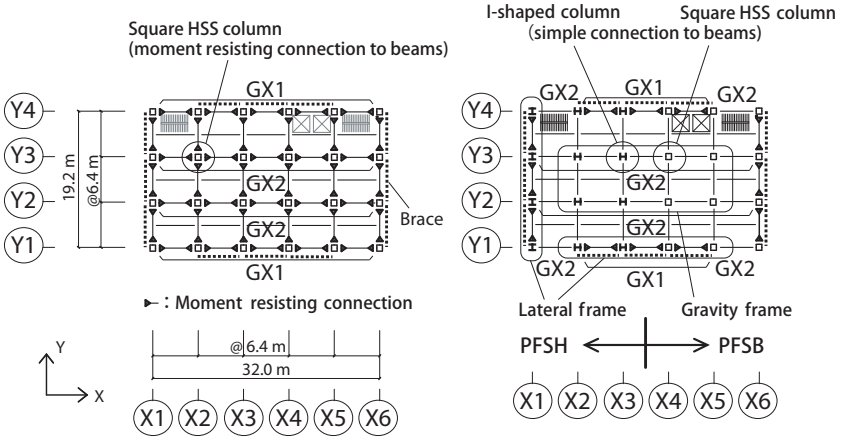

Figure 1. Floor framing plan

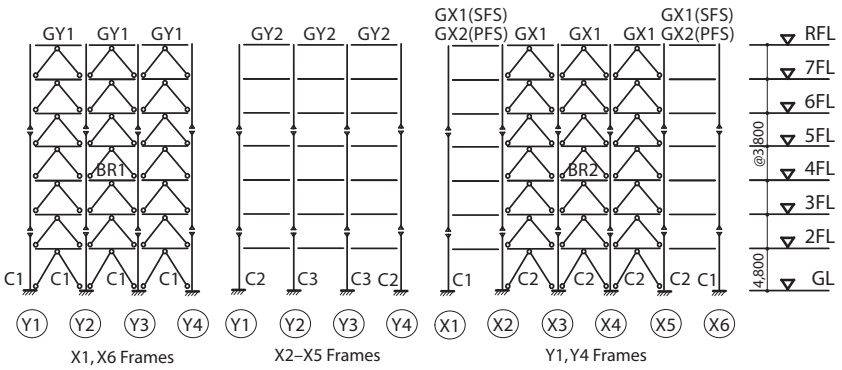

Figure 2. Framing elevations

Table 1. Member grouping in stories

Part	Columns	Beams	Braces
3	Mid. 5th Flr.-7th Flr.	6th Flr.-Roof	5th Flr.-7th Flr.
2	Mid. 2nd Flr.-Mid. 5th Flr.	3rd Flr.-5th Flr.	2nd Flr.-4th Flr.
1	1st Flr.-Mid. 2nd Flr.	2nd Flr.	1st Flr.

the responses in preliminary response history analyses under the same conditions described below. C_{QUN1} is determined in the sequence of multiple preliminary analyses. The member sections in the final operation of preliminary analysis are not exactly the same as those in the superior solutions obtained below but they are close.

There are two reasons that C_{QUN1} is defined based not only on the code but also by referring to the response history analyses: (1) In the case of using the code-required C_{QUN1}, the requirement of the ultimate lateral strength is not the dominant design condition for the moment-frame system, and consequently the ultimate lateral strength of SFS is greater than that of PFS. Therefore, the design solutions of SFS and PFS do not have the equivalent seismic performance. (2) By using design solutions based on seismic responses, structural characteristics of different building structures (moment or braced frame) as well as structural systems (SFS or PFS) can be compared under consistent seismic design criteria against very rare (L2) earthquakes.

3. Superior Design Solutions by MSLS

3.1 Algorithm to obtain the superior solutions

Superior design solutions of SFS, PFSB, and PFSH are obtained by the MSLS method.[13] The design variables are discrete section sizes under the conditions of the first and second design constraints. The objective function to be minimized is the steel volume. Feasible solutions, which satisfy all constraints, are first obtained from approximately 10^7 random combinations of design variables. In the next step, the 10 best feasible solutions are assigned as initial solutions for MSLS. The superior solutions are defined as the best local optimal solutions obtained from the 10 different initial solutions. There are approximately 40 variables representing the section sizes, and approximately 100 complex constraints. Because the ratio of combinations satisfying all constraints to randomly generated combinations is very small at 10^{-5} to 10^{-4}, probabilistic approaches such as the genetic algorithm are not effective to solve this problem.

A step-by-step algorithm is assumed in MSLS. In the process, from a randomly generated initial solution to a local optimal solution, neighborhood solutions are examined around a tentative solution at each step. The number of neighborhood solutions examined is set as the same as the number of variables. In the case that the objective function is improved, and all constraints are satisfied in the best neighborhood solution, then the tentative solution is replaced. When no better solution is found in the neighborhood, the tentative solution is carried over to the next step. Discrete variables of section sizes are randomly increased or decreased by one or stay the same within the range of each variable. The number of steps is set as 3000. Therefore, the total number of neighborhood solutions is approximately $3000 \times 40 = 120\,000$. The constraints such as the width-to-thickness ratio are checked first without analyses and approximately 1/5 of the neighborhood solutions is analyzed.

The superior solutions are not globally optimal solutions; however, they are rationally obtained in the specified design algorithm independent of engineers' experience or preference. This research aims at identifying structural characteristics of steel frames with different building structures and structural systems by comparing the superior solutions. Therefore, obtaining strictly global optimal solutions is not the primary interest of this research. The superior solutions shown below can be improved, if the number of steps is increased; however, the decrease in steel volume in the superior solutions with 30 000 steps in MSLS is less than 1%. Development of more effective algorithm may be a possible future direction of this research.

3.2 3D frame model

Three-dimensional (3D) frame models are created for the elastic analyses for the first design step and the inelastic pushover analyses for the second design step. The modeling assumptions are essentially the same as in the previous work[8] and are summarized in Appendix 2. The ultimate lateral strength calculated in inelastic pushover analyses is defined for the moment frames as the story shear force at which the maximum interstory drift first reaches 1.25%. Additionally, it is defined as the story shear force for braced frames when the compressive axial forces first reach the buckling strength, which is assumed as 1.1 times the product of allowable temporary compressive stress and the cross-sectional area.

The buckling strength of beams is defined as the average of the tensile yield strength and buckling strength around the weak axis, by assuming that the upper flange of the beam is

Table 2. Discrete MSLS variables

Symbols	Members	Parts	Discrete variable options
D_c	Rectangular HSS columns	Width	Every 50 mm in 250-800 mm
t_c		Thickness	(excluding 9 mm)[a]
H_{wc}	I-shaped columns	Height	Every 50 mm in 300-900 mm
W_{fc}		Flange width	Every 50 mm in 300-700 mm
t_{wc}		Web thickness	[a]
t_{fc}		Flange thickness	(excluding 9 and 12 mm)[a]
H_w	Beams	Height	Every 50 mm in 300-1000 mm
W_f		Flange width	Every 50 mm in 200-400 mm[b]
t_w		Web thickness	[a]
t_f		Flange thickness	[a,b]
D_p	Braces	Diameter	318.5, 355.6, 406.4, 457.2 mm
t_p		Thickness	(including 6 mm)[a]

	1	2	3	4	5	6	7	8	9	10	11	12
W_f (mm^2)	150	150	200	200	250	250	250	300	300	300	350	350
t_f (mm^2)	12	16	16	19	19	22	25	25	28	32	32	36
A_f (10^3 mm^2)	1.8	2.4	3.2	3.8	4.8	5.5	6.3	7.5	8.4	9.6	11.1	12.6

[a]Plate thickness options are 9, 12, 16, 19, 22, 25, 28, 32, 36, and 40 mm. [b]Combinational options of the flange width and thickness in beams are shown below.

constrained by the slab and the lower flange is not. The axial forces of the beams are calculated as half of the sum of shear forces of inverted-V shaped concentrated braces, which are supposed to be transferred by the axial force of the connecting beams. The buckling lengths are assumed as the member lengths between the connecting nodes.

An in-house code is used for the elastic analysis and inelastic pushover analysis for the MSLS. The accuracy has been verified in comparison to the results by a commercial analysis software Midas.[14] The number of degrees of freedom in the 3D frame models is 1000-2000, and the computation time of single MSLS operation is varied in 50-200 minutes by a PC with Intel Xeon W-2125 processor, 4.00 GHz, with 24 GB memory. The computation time depends on the size of the model and ratio of acceptance of the best neighborhood solution at each step.

3.3 Variables and constraints

The discrete variables of section sizes are similarly defined as those in the authors' previous work.[8] Possible ranges of the variables are shown in Table 2. These variables of section sizes are defined from the list of standard rolled sections[15] and built-up sections with steel plates with standard thickness. The discrete width and height of the sections in the columns and beams are defined every 50 mm. The thickness of standard round HSSs is varied with the diameters and may not be the same as the standard plate thickness; however, for the sake of simplicity, the set of thicknesses of the round HSSs is assumed to be the same as the set of standard plate thicknesses. The combinations of the flange width and thickness are defined as shown in Table 2, where the cross-sectional area of flange A_f is considered as an independent variable.

The constraints of MSLS are similar to those in the previous work,[8] which are summarized in Appendix 3. GX2 and GY2 beams are supported in pins at their ends as shown in Figures 1 and 2, and have the section H-400 × 200 × 8 × 13, which is the minimum I-shaped rolled section carrying the gravity load, and the section size of GX2 and GY2 is excluded from the variables.

4. Evaluation of Superior Solutions

4.1 MSLS analysis result

Tables 3 and 4 show the section sizes in the superior solutions of SFS, PFSH, and PFSB, with $C_{QUN1} = 0.6$ for the moment-frame structures and $C_{QUN1} = 1.0$ for the braced-frame structures. 3D inelastic frame models are created for these solutions, using Midas.[14] "Stress ratios" are defined as ratios of stresses under the first design step loads to the allowable stresses. The design temporary load is the combined gravity (dead plus live load) and seismic load with 0.2 of the base-shear coefficient. The values of the stress ratios are shown in parentheses. "X," "Y," and "L" shown in square brackets indicate that the dominant load is the temporary load with the seismic load in the X- or Y-direction (hereinafter, these loads are referred to as "X load" and "Y load") or the gravity load, respectively.

Figure 3 shows the relationships between the base-shear coefficient and inter-story drift ratio in the first story obtained by the pushover analyses using Midas.[14] The filled circle and cross marks in the plot indicate the ultimate lateral strength of moment- and braced-frame structures, respectively. Most of the base-shear coefficient of the ultimate lateral strength C_{QU1} is greater than $C_{QUN1} = 0.6$ for the moment frames and $C_{QUN1} = 1.0$ for the braced frames. In order to save on computational cost, no iterative calculation is performed in each step of load increment in the pushover algorithm in MSLS, which is different from the algorithm in Midas. Consequently, C_{QU1} obtained by Midas is slightly smaller than $C_{QUN1} = 0.6$ for the moment frames; however, the shortage is less than 2%. As Figure 3 shows, the values of C_{QU1} and C_{QUN1} are close. Therefore, the constraints for the ultimate lateral strength substantially influence the superior solutions. $C_{QUN1} = 0.6$ for the moment frame and $C_{QUN1} = 1.0$ for the braced frame are 2.0 and 2.9 times as much as $C_{QUN1} = 0.3$ for the moment frame and $C_{QUN1} = 0.35$ for the braced frame of the code-required values. Therefore, the temporary X and Y loads are not dominant for the seismic design. The maximum inter-story drift ratios are 0.29%-0.36% (PFSB-SFS) for the moment-frame

Table 3. Superior solutions of moment-frame structures (C_{QUN1} = 0.6)

SFS

Part	C1	C2	C3
3	BX-550 × 550 × 19 (0.25)[Y]	BX-450 × 450 × 16 (0.36)[X]	BX-500 × 500 × 16 (0.35)[X]
2	BX-550 × 550 × 19 (0.37)[Y]	BX-450 × 450 × 19 (0.49)[Y]	BX-500 × 500 × 22 (0.49)[Y]
1	BX-550 × 550 × 22 (0.56)[X]	BX-450 × 450 × 28 (0.52)[Y]	BX-500 × 500 × 32 (0.50)[Y]

Part	GX1	GX2	GY1	GY2
3	H-550 × 200 × 12 × 16 (0.59)[X]	H-550 × 200 × 12 × 19 (0.60)[X]	H-550 × 200 × 12 × 19 (0.61)[Y]	H-550 × 200 × 12 × 16 (0.63)[Y]
2	H-700 × 200 × 12 × 16 (0.61)[X]	H-700 × 300 × 12 × 25 (0.51)[X]	H-700 × 250 × 12 × 19 (0.55)[Y]	H-700 × 300 × 12 × 25 (0.45)[Y]
1	H-700 × 250 × 12 × 25 (0.53)[X]	H-700 × 250 × 12 × 25 (0.57)[X]	H-700 × 200 × 12 × 16 (0.65)[Y]	H-700 × 300 × 12 × 32 (0.43)[Y]

PFSH

Part	C1	C2	C3
3	H-850 × 300 × 25 × 22 (0.52)[Y]	H-900 × 300 × 25 × 22 (0.50)[X]	H-400 × 350 × 12 × 22 (0.26)[L]
2	H-850 × 450 × 25 × 40 (0.49)[Y]	H-900 × 450 × 25 × 36 (0.51)[X]	H-400 × 300 × 12 × 22 (0.62)[L]
1	H-850 × 650 × 25 × 40 (0.56)[Y]	H-900 × 650 × 25 × 32 (0.64)[X]	H-400 × 300 × 12 × 22 (0.82)[L]

Part	GX1	GX2	GY1	GY2
3	H-800 × 300 × 16 × 28 (0.49)[X]	H-400 × 200 × 8 × 13 (0.90)[L]	H-850 × 250 × 16 × 25 (0.55)[Y]	H-400 × 200 × 8 × 13 (0.90)[L]
2	H-1000 × 350 × 19 × 36 (0.49)[X]	H-400 × 200 × 8 × 13 (0.90)[L]	H-1000 × 350 × 19 × 36 (0.49)[Y]	H-400 × 200 × 8 × 13 (0.90)[L]
1	H-900 × 350 × 16 × 32 (0.54)[X]	H-400 × 200 × 8 × 13 (0.90)[L]	H-900 × 350 × 16 × 36 (0.53)[Y]	H-400 × 200 × 8 × 13 (0.90)[L]

PFSB

Part	C1	C2	C3
3	BX-650 × 650 × 22 (0.37)[Y]	BX-700 × 700 × 25 (0.30)[X]	BX-300 × 300 × 16 (0.27)[L]
2	BX-650 × 650 × 32 (0.48)[Y]	BX-700 × 700 × 25 (0.50)[X]	BX-300 × 300 × 19 (0.45)[L]
1	BX-650 × 650 × 32 (0.50)[Y]	BX-700 × 700 × 28 (0.54)[X]	BX-300 × 300 × 16 (0.65)[L]

Part	GX1	GX2	GY1	GY2
3	H-800 × 300 × 16 × 25 (0.54)[X]	H-400 × 200 × 8 × 13 (0.90)[L]	H-900 × 250 × 16 × 22 (0.56)[Y]	H-400 × 200 × 8 × 13 (0.90)[L]
2	H-950 × 350 × 19 × 36 (0.51)[X]	H-400 × 200 × 8 × 13 (0.90)[L]	H-1000 × 350 × 19 × 36 (0.51)[Y]	H-400 × 200 × 8 × 13 (0.90)[L]
1	H-900 × 400 × 16 × 36 (0.48)[X]	H-400 × 200 × 8 × 13 (0.90)[L]	H-1000 × 300 × 19 × 25 (0.60)[Y]	H-400 × 200 × 8 × 13 (0.90)[L]

structures and 0.08%-0.09% (PFSH-SFS) for the braced-frame structures. These values are smaller than the first design step requirement of 0.5%. Moreover, the maximum stress ratios are relatively small, and are 0.60-0.65 (PFSB-SFS) for the moment-frame structures and 0.32-0.34 (PFSB-PFSH) for the braced-frame structures.

4.2 Response history analyses

Response history analyses are performed for the superior solutions in order to evaluate their dynamic behaviors. The commercial analysis software SNAP[16] is used for the numerical simulations. The analysis models are essentially the same as those for the static pushover analyses. First natural periods are

Table 4. Superior solutions of braced-frame structures (C_{QUN1} = 1.0)

SFS Part	C1	C2	C3	BR1	BR2
3	BX-350 × 350 × 12 (0.33)[L]	BX-350 × 350 × 16 (0.36)[L]	BX-250 × 250 × 28 (0.26)[L]	P-406.4 × 9 (0.22)[Y]	P-318.5 × 12 (0.23)[X]
2	BX-350 × 350 × 28 (0.30)[Y]	BX-350 × 350 × 28 (0.34)[X]	BX-250 × 250 × 16 (0.70)[L]	P-318.5 × 19 (0.21)[Y]	P-355.6 × 16 (0.21)[X]
1	BX-350 × 350 × 40 (0.31)[Y]	BX-350 × 350 × 40 (0.32)[X]	BX-250 × 250 × 19 (0.72)[L]	P-355.6 × 19 (0.21)[Y]	P-406.4 × 16 (0.20)[X]

Part	GX1	GX2	GY1	GY2
3	H-300 × 250 × 9 × 19 (0.32)[L]	H-300 × 200 × 9 × 16 (0.64)[L]	H-300 × 200 × 9 × 19 (0.05)[Y]	H-300 × 200 × 9 × 16 (0.65)[L]
2	H-400 × 200 × 12 × 19 (0.27)[X]	H-400 × 200 × 9 × 16 (0.49)[L]	H-400 × 200 × 12 × 19 (0.09)[Y]	H-400 × 200 × 9 × 16 (0.49)[L]
1	H-350 × 200 × 12 × 16 (0.33)[L]	H-350 × 200 × 9 × 19 (0.41)[L]	H-350 × 350 × 12 × 36 (0.09)[Y]	H-350 × 200 × 9 × 16 (0.46)[L]

PFSH Part	C1	C2	C3	BR1	BR2
3	H-800 × 300 × 22 × 19 (0.16)[Y]	H-600 × 300 × 16 × 25 (0.19)[X]	H-450 × 300 × 12 × 28 (0.25)[L]	P-457.2 × 9 (0.20)[Y]	P-457.2 × 9 (0.20)[X]
2	H-800 × 450 × 22 × 25 (0.28)[Y]	H-600 × 500 × 16 × 28 (0.30)[X]	H-450 × 300 × 12 × 25 (0.55)[L]	P-457.2 × 12 (0.21)[Y]	P-457.2 × 12 (0.21)[X]
1	H-800 × 600 × 22 × 32 (0.33)[Y]	H-800 × 550 × 16 × 40 (0.34)[X]	H-450 × 300 × 12 × 32 (0.59)[L]	P-355.6 × 16 (0.23)[Y]	P-457.2 × 12 (0.22)[X]

Part	GX1	GX2	GY1	GY2
3	H-350 × 250 × 12 × 19 (0.06)[X]	H-400 × 200 × 8 × 13 (0.90)[L]	H-300 × 250 × 9 × 19 (0.05)[Y]	H-400 × 200 × 8 × 13 (0.90)[L]
2	H-300 × 250 × 9 × 25 (0.08)[X]	H-400 × 200 × 8 × 13 (0.90)[L]	H-300 × 250 × 9 × 22 (0.08)[Y]	H-400 × 200 × 8 × 13 (0.90)[L]
1	H-450 × 250 × 12 × 25 (0.16)[X]	H-400 × 200 × 8 × 13 (0.90)[L]	H-550 × 300 × 16 × 32 (0.16)[Y]	H-400 × 200 × 8 × 13 (0.90)[L]

PFSB Part	C1	C2	C3	BR1	BR2
3	BX-350 × 350 × 16 (0.15)[Y]	BX-350 × 350 × 19 (0.15)[X]	BX-300 × 300 × 12 (0.35)[L]	P-457.2 × 9 (0.20)[Y]	P-355.6 × 12 (0.21)[X]
2	BX-350 × 350 × 28 (0.28)[Y]	BX-350 × 350 × 32 (0.27)[X]	BX-300 × 300 × 12 (0.70)[L]	P-457.2 × 12 (0.21)[Y]	P-318.5 × 22 (0.19)[X]
1	BX-350 × 350 × 40 (0.32)[Y]	BX-350 × 350 × 40 (0.30)[X]	BX-300 × 300 × 25 (0.43)[L]	P-457.2 × 12 (0.23)[Y]	P-406.4 × 28 (0.13)[X]

Part	GX1	GX2	GY1	GY2
3	H-300 × 250 × 9 × 19 (0.04)[X]	H-400 × 200 × 8 × 13 (0.90)[L]	H-300 × 200 × 9 × 16 (0.05)[Y]	H-400 × 200 × 8 × 13 (0.90)[L]
2	H-300 × 250 × 9 × 19 (0.07)[X]	H-400 × 200 × 8 × 13 (0.90)[L]	H-350 × 250 × 12 × 19 (0.09)[Y]	H-400 × 200 × 8 × 13 (0.90)[L]
1	H-350 × 250 × 12 × 22 (0.10)[X]	H-400 × 200 × 8 × 13 (0.90)[L]	H-500 × 250 × 16 × 22 (0.13)[Y]	H-400 × 200 × 8 × 13 (0.90)[L]

shown in Table 5. While post-buckling behavior is not simulated in the pushover analyses, it is incorporated in the response history analyses. The force recovery relationships against axial force are defined based on the study by Shibata et al.[17–19] The damping factor h is given as 2.0% based on the instantaneous stiffness.

Very rare earthquake ground motions (L2 earthquakes) are used for the response history analyses. Recorded ground motions from three events, El Centro NS (1940), Taft EW (1952), and Kobe (JMA) NS (1995), are scaled to the maximum velocity of 500 mm/s. Figure 4 shows the acceleration response spectrum (h = 2%) of these L2 earthquakes. The

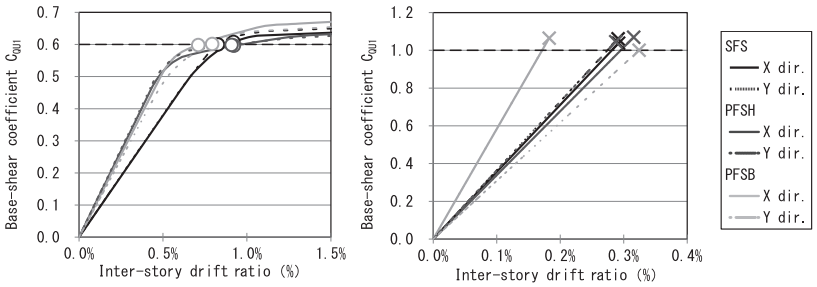

Figure 3. Relationships between base-shear coefficient and inter-story drift ratio of moment- and braced-frame structures

Table 5. First natural periods of superior solutions (s)

		SFS		PFSH		PFSB	
		X	Y	X	Y	X	Y
Moment frame structures	C_{QUN1} = 0.3	1.30	1.28	1.23	1.31	1.21	1.25
	C_{QUN1} = 0.6	1.05	1.05	0.92	0.92	0.96	0.96
Braced frame structures	C_{QUN1} = 0.35	0.76	0.79	0.74	0.78	0.80	0.79
	C_{QUN1} = 1.0	0.49	0.49	0.50	0.49	0.46	0.51
BRB structures C_{QUN1} = 0.5	P = 1.0	0.66	0.66	0.67	0.66	0.67	0.66
	P = 5.0	0.69	0.72	0.69	0.70	0.69	0.69
Mixed structures C_{QUN1X} = 0.6 C_{QUN1Y} = 1.0		1.00	0.45	0.85	0.47	0.88	0.46

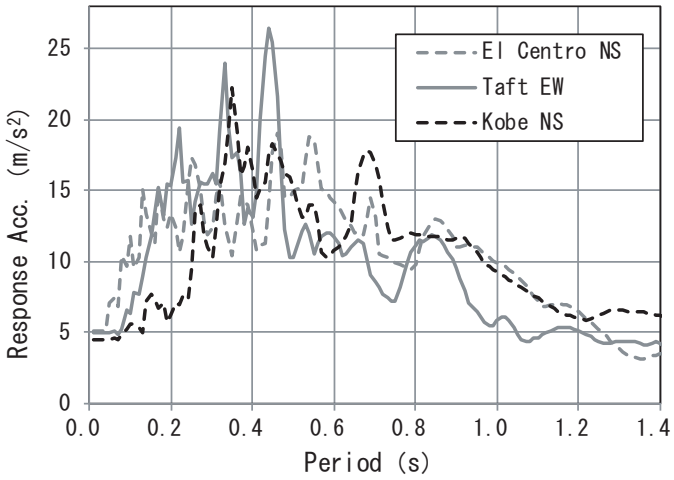

Figure 4. Acceleration response spectra of ground motions (h = 2%)

duration of the analyses is set as 60 seconds and the time increment is 1/200 seconds. The Newmark β method (β = 1/4) is used for time integration.

4.3 Responses

4.3.1 Moment-frame structures

Only the results of the El Centro and Kobe earthquakes, which have large responses, are shown in the following. The maximum story shear coefficient C_{MAX} and inter-story drift ratio R_{MAX} are shown in Figures 5 and 6, respectively. The vertical distribution factor A_i used in the pushover analyses is shown in Figure 5, which mostly agrees with the distribution of the maximum story shear coefficients. The maximum base-shear coefficient C_{MAX1} is 0.54-0.57 for the moment-frame structures, and the difference among the three structural systems is relatively small. The base-shear coefficient of the required ultimate lateral strength C_{QUN1} is defined as 0.6 for MSLS, which is based on the values of C_{MAX1}. C_{MAX} could be reduced, if the structures were designed more flexibly. However, preliminary study showed that strength became insufficient in the more flexible structures. Therefore, it is reasonable to define C_{QUN1} as 0.6, corresponding to the structural design against L2 earthquakes. However, the maximum value of R_{MAX} in the X- and Y-directions is 1.43% in SFS and 1.41% in PFSH. Furthermore, the maximum ductility factors are 2.46 in SFS, 2.84 in PFSH, and 2.85 in PFSB, where the ductility factor is defined as the ratio of the maximum member rotation to member rotation at yielding. The concentration of large inelastic deformation is not observed in particular members, and plastic hinges are distributed over the frames. The maximum residual inter-story drift ratio is 0.37%.

4.3.2 Braced-frame structures

C_{MAX1} obtained by response history analyses has large value 1.04-1.25 for the braced-frame structures. This is because the first natural periods are 0.46-0.51 seconds, which are shorter than those of moment-frame structures, 0.92-1.05 seconds, and there is less energy dissipation by inelastic deformations in the braced-frame structures. R_{MAX} is slightly larger than 1.0% in PFSB under El Centro L2 earthquake as shown in Figure 6.

4.3.3 Ultimate lateral strength calculation and response history analysis

In Japan, commonly adopted structural design criteria in response history analysis against L2 earthquakes are 1.0% for the maximum inter-story drift ratio and 4.0 for the maximum ductility factor. The superior solutions for the moment frames under C_{QUN1} = 0.6 satisfy the criteria on the ductility factor but do not on the inter-story drift ratio. C_{QUN1} is defined as 1.0 for the superior solutions for the braced-frame structures, while the code-required value can be as small as 0.35. Additionally, the superior solutions under C_{QUN1} = 1.0 do not necessarily satisfy the practical common design criteria using response history analyses against L2 earthquakes.

Seven-story office buildings examined in this research can be designed using either the pushover or response history analyses in Japan. It is found through the simulations that the "L2 design," which satisfies the requirements in the response history analysis against L2 earthquakes, is significantly stronger than the "Q_{UN} design," which satisfies the requirements in the pushover calculations. The superior solutions for moment-frame structures with C_{QUN1} = 0.3 satisfy the Q_{UN} design

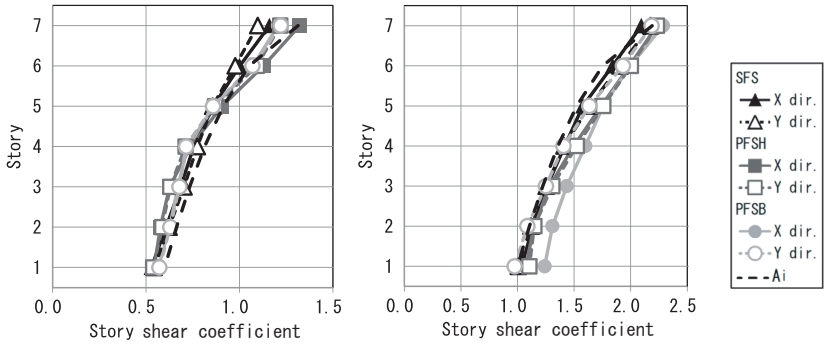

Figure 5. Maximum shear coefficient (El Centro)

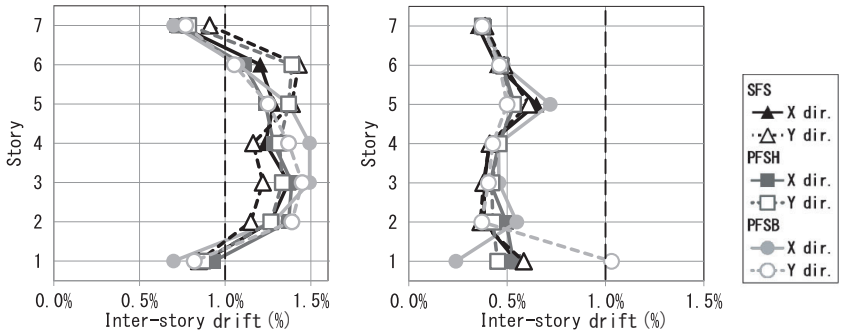

Figure 6. Maximum inter-story drift ratio

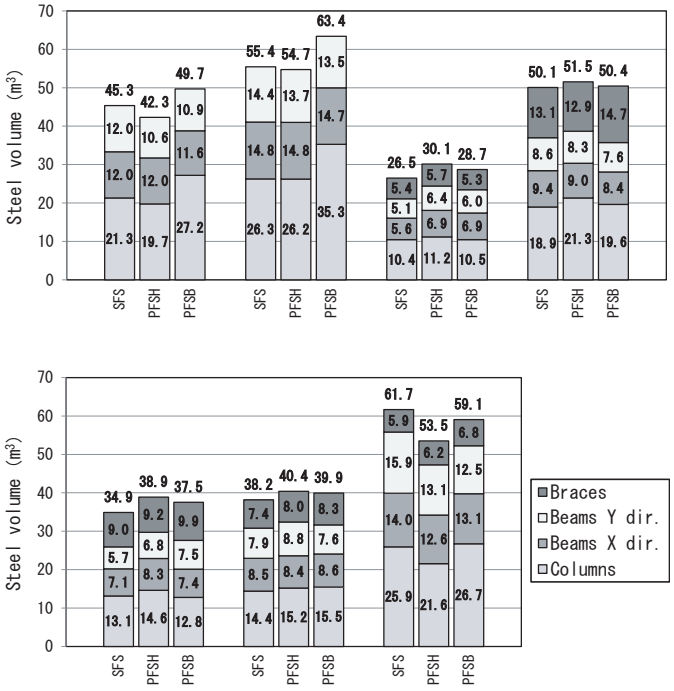

Figure 7. Comparison of steel volume

criteria; however, those with $C_{QUN1} = 0.6$ may not satisfy the L2 design criteria. Additionally, the superior solutions for braced-frame structures with $C_{QUN1} = 0.35$ satisfy the Q_{UN} design criteria; however, those with $C_{QUN1} = 1.0$ may not satisfy the L2 design criteria. Similar characteristics can be observed in buildings with relatively short natural periods. Thus, the difference of the seismic performance required for the ultimate lateral strength calculations and response history analyses has been quantitatively evaluated.

4.4 Steel volume

The steel volumes of the superior solutions shown in Tables 3 and 4 are compared in Figure 7. Furthermore, the steel volumes for the superior solutions of moment-frame structures with $C_{QUN1} = 0.3$ and braced-frame structures with $C_{QUN1} = 0.35$ are shown in Figure 7.

4.4.1 Moment-frame structures

The superior solutions of moment-frame structures with $C_{QUN1} = 0.3$ are primarily controlled by the constraints of the allowable stress design including the limitation of the inter-story drift ratio (0.5%), whereas those with $C_{QUN1} = 0.6$ are primarily controlled by the constraints of the ultimate lateral strength. The steel volumes are smaller, in the order of PFSH, SFS, and PFSB, both with $C_{QUN1} = 0.3$ and 0.6. The steel volumes with $C_{QUN1} = 0.6$ are 22%-29% greater than those with $C_{QUN1} = 0.3$. The section of secondary beams is assigned as H-400 × 200 × 8 × 13 and 30% more steel is included for miscellaneous parts such as stiffeners and brackets for exteriors. The total steel weight per unit area (kg/m^2) is 113.0 (SFS), 106.2 (PFSH), and 122.6 (PFSB) with $C_{QUN1} = 0.3$, and 135.4 (SFS), 133.8 (PFSH), and 153.2 (PFSB) with $C_{QUN1} = 0.6$. The steel volumes of PFSH are smaller because the column strength and stiffness can be adjusted with fewer restrictions by changing the I-shaped column section sizes. Additionally, it is effective for limited lateral frames to carry the seismic loads. In SFS, the height of beams in each floor is assumed to be uniform; however, this constraint has little

effect on the increase in the steel volume, mainly because column spacing is uniform in both the X- and Y-directions. In this study, yielding of panels in I-shaped columns is not simulated and additional steel plates reinforcing the panels may be required; however, their steel volume would be limited with respect to the total volume. Considering that the steel volume of the horizontal stiffeners at the beam-to-column connections in the rectangular HSS column is not taken into account, detailed evaluation for the volume of reinforcing plates for the panels is not necessary. Because the ultimate lateral strengths of the superior solutions with $C_{QUN1} = 0.6$ are almost the same among SFS, PFSH, and PFSB, and the maximum inter-story drift ratios and ductility factors are not significantly different. Hence, PFSH can be advantageous with less steel volume.

Automated fabrication technology for connections with rectangular HSS columns has been developed and widely used in Japan. The quality and productivity of complete-joint-penetration (CJP) groove welding are high; however, the amount of welding in the beam-to-column connections is also large.[7] Therefore, the advantages of PFSH using I-shaped columns, where CJP welding is not required in the beam-to-column connections, may be worth for further consideration. However, the steel volume of PFSB is greater than those of SFS and PFSH. The steel volume in columns is greater in PFSB and this difference directly results in the difference in total steel volume. Thus, disadvantage of using rectangular HSS columns in one-way moment frames has been quantitatively evaluated.

4.4.2 Braced-frame structures

Contrary to the moment-frame structures, the primary forces induced by the seismic load in braced-frame structures are axial forces. Therefore, the difference in steel volume among the structural systems, SFS, PFSH, and PFSB, is relatively small. Since I-shaped columns are disadvantageous against buckling, and the steel volume in PFSH is slightly larger as shown in Figure 7.

Braces carry most of the seismic lateral load in the braced-frame structures, and therefore the sizes of members in the gravity frames (C3, GX2, and GY2 in Figures 1 and 2) are not controlled by the seismic loads. When the beams are designed for the gravity load, mid-span flexural moments and deflections are smaller with moment connections to the columns, but there is less composite effect with the floor slabs. Beam cambers are commonly used in steel buildings in the United States and other countries but not in Japan. The composite effect and cambers are not considered in this research. The superior design algorithm against the gravity load can be improved in future research.

The column spacing of 6.4 m is shorter than that in standard office buildings, and the beam sections are small. Consequently, the strong-column-weak-beam constraint has little effect on increase in column sections. This may partly account for the less significant difference between SFS and PFS. Increasing the column spacing from 6.4 to 9.6 m, the steel volume in SFS becomes slightly less than the others. Compared to PFSB, the advantage of decreasing steel in beams by moment connections to columns outweighs the disadvantage of increasing column sections under the strong-column-weak-beam constraint.

The steel volumes of the superior solutions with $C_{QUN1} = 1.0$ are 70%-90% larger than those with $C_{QUN1} = 0.35$. The steel weight per unit area (kg/m^2) calculated in the similar manner as the moment-frame structures is 68.3 (SFS), 76.2 (PFSH), and 73.3 (PFSB) with $C_{QUN1} = 0.35$, and is 116.8 (SFS), 120.2 (PFSH), and 116.8 (PFSB) with $C_{QUN1} = 1.0$.

5. Buckling Restrained Braces

In the previous section, the base-shear coefficient of required ultimate lateral strength C_{QUN1} is defined as 1.0 for the superior solutions with braced-frame structures, referring to the responses in response history analyses against very rare (L2) earthquakes. Consequently, the sizes of members including braces in the superior solutions are large. In this section, superior solutions using buckling restrained braces (BRB) are obtained for the three structural systems: SFS, PFSH, and PFSB. It is confirmed that the C_{QUN1} value for the BRB structures is reduced by the energy dissipation by BRBs. Consequently, members in the BRB structures become smaller. The seismic behavior of the BRB structures is also examined.

5.1 Modeling of BRB

In this section, modeling of BRBs and the objective function of steel volume including BRBs are described. The force restoring characteristics of BRBs are normal bilinear and symmetric in the tensile and compressive directions. The initial stiffness, post-yielding stiffness, and yielding strength are denoted as K_{1BRB}, K_{2BRB}, and N_{YBRB}, respectively. The axial stiffness of BRBs and connecting elements are both taken into account for K_{1BRB} and K_{2BRB}. K_{2BRB} is defined as 0.01 K_{1BRB}, and a linear relationship between K_{1BRB} and N_{YBRB} is assumed as shown in Equation (1). This creates one variable for one BRB. The values of N_{YBRB} are selected every 500 kN between 1000 and 3500 kN.

$$K_{1BRB} = \alpha N_{YBRB} \tag{1}$$

K_{1BRB} is calculated using information of the axial stiffness of BRBs[20,21] and connecting elements, which are designed for each N_{YBRB}. The average ratio of K_{1BRB}-N_{YBRB} is 0.19 (1/mm) and it is denoted by the constant α. Although the height of the first story is 4.8 m and higher than the 3.8 m of other stories as shown in Figure 2, Equation (1) is valid for the BRBs in the first story. This is because the axial stiffness of BRBs is lower than that of the connecting elements and the length of the connecting elements does not significantly affect K_{1BRB}. Furthermore, the total weight of BRB and connecting elements denoted by W_{BRB} is almost proportional to N_{YBRB}. Therefore, the following relationship in the steel volume of BRBs is obtained:

$$W_{BRB}/\rho = a_1 N_{YBRB} L \tag{2}$$

where $\rho = 7.85$ ton/m^3 is the specific weight of steel, L is the total length of BRBs and the connecting elements (distance between the connecting two nodes in the simulation models), and a_1 is a coefficient defined as 6.5×10^{-6} m^2/kN. The right-hand side of Equation (2) is the equivalent steel volume of BRB, V_{EBRB}. In the investigation below, the product of P and V_{EBRB} is included in the objective function, where P is the cost coefficient. In the case where the cost of BRBs is relatively low and nearly equal to that of regular steel, 1.0 is assumed for P. Contrarily, in the case where the cost of BRBs is high, 5.0 is assumed in the MSLS calculations. Referring to preliminary response history analyses, C_{QUN1} is defined as 0.5.

5.2 Superior solutions for BRB structures

The superior solutions of BRB structures with $P = 5.0$ are shown in Table 6. The yielding strength N_{YBRB} is shown for

Table 6. Superior solutions of BRB structures (P = 5.0)

SFS Part	C1	C2	C3	BRB1	BRB2
3	BX-400 × 400 × 16 (0.19)[Y]	BX-350 × 350 × 12 (0.43)[L]	BX-300 × 300 × 16 (0.29)[Y]	N_{YBRB} = 1000 kN (0.69)[Y]	N_{YBRB} = 1000 kN (0.68)[X]
2	BX-400 × 400 × 16 (0.42)[Y]	BX-350 × 350 × 12 (0.68)[X]	BX-300 × 300 × 16 (0.53)[L]	N_{YBRB} = 1500 kN (0.65)[Y]	N_{YBRB} = 1500 kN (0.64)[X]
1	BX-400 × 400 × 16 (0.62)[Y]	BX-350 × 350 × 25 (0.48)[X]	BX-300 × 300 × 25 (0.44)[L]	N_{YBRB} = 1500 kN (0.71)[Y]	N_{YBRB} = 2000 kN (0.55)[X]

Part	GX1	GX2	GY1	GY2
3	H-300 × 150 × 9 × 16 (0.55)[L]	H-300 × 250 × 9 × 22 (0.40)[L]	H-300 × 150 × 9 × 12 (0.11)[Y]	H-300 × 200 × 9 × 16 (0.57)[L]
2	H-400 × 200 × 12 × 16 (0.42)[X]	H-400 × 150 × 9 × 12 (0.64)[L]	H-400 × 250 × 12 × 19 (0.16)[Y]	H-400 × 150 × 9 × 16 (0.50)[L]
1	H-450 × 150 × 12 × 16 (0.34)[X]	H-450 × 150 × 9 × 16 (0.42)[L]	H-450 × 200 × 12 × 16 (0.26)[Y]	H-450 × 250 × 9 × 25 (0.22)[Y]

PFSH Part	C1	C2	C3	BRB1	BRB2
3	H-600 × 300 × 16 × 28 (0.18)[Y]	H-600 × 300 × 16 × 19 (0.25)[X]	H-350 × 300 × 12 × 16 (0.41)[L]	N_{YBRB} = 1000 kN (0.73)[Y]	N_{YBRB} = 1000 kN (0.70)[X]
2	H-600 × 350 × 16 × 22 (0.47)[Y]	H-600 × 450 × 16 × 25 (0.36)[X]	H-350 × 300 × 12 × 16 (0.82)[L]	N_{YBRB} = 1500 kN (0.66)[Y]	N_{YBRB} = 1500 kN (0.66)[X]
1	H-600 × 400 × 16 × 28 (0.54)[Y]	H-600 × 400 × 16 × 32 (0.53)[X]	H-350 × 350 × 12 × 19 (0.77)[L]	N_{YBRB} = 2500 kN (0.45)[Y]	N_{YBRB} = 2500 kN (0.45)[X]

Part	GX1	GX2	GY1	GY2
3	H-300 × 150 × 9 × 16 (0.12)[X]	H-400 × 200 × 8 × 13 (0.90)[L]	H-300 × 250 × 9 × 25 (0.11)[Y]	H-400 × 200 × 8 × 13 (0.90)[L]
2	H-450 × 250 × 12 × 25 (0.18)[X]	H-400 × 200 × 8 × 13 (0.90)[L]	H-500 × 250 × 16 × 25 (0.19)[Y]	H-400 × 200 × 8 × 13 (0.90)[L]
1	H-300 × 250 × 9 × 19 (0.19)[X]	H-400 × 200 × 8 × 13 (0.90)[L]	H-300 × 200 × 9 × 19 (0.20)[Y]	H-400 × 200 × 8 × 13 (0.90)[L]

PFSB Part	C1	C2	C3	BRB1	BRB2
3	BX-350 × 350 × 12 (0.24)[Y]	BX-400 × 400 × 16 (0.18)[X]	BX-300 × 300 × 16 (0.27)[L]	N_{YBRB} = 1000 kN (0.71)[Y]	N_{YBRB} = 1000 kN (0.71)[X]
2	BX-350 × 350 × 16 (0.47)[Y]	BX-400 × 400 × 22 (0.33)[X]	BX-300 × 300 × 12 (0.70)[L]	N_{YBRB} = 2000 kN (0.53)[Y]	N_{YBRB} = 2000 kN (0.53)[X]
1	BX-350 × 350 × 25 (0.51)[Y]	BX-400 × 400 × 25 (0.49)[X]	BX-300 × 300 × 16 (0.65)[L]	N_{YBRB} = 1500 kN (0.72)[Y]	N_{YBRB} = 1500 kN (0.71)[X]

Part	GX1	GX2	GY1	GY2
3	H-350 × 150 × 12 × 16 (0.13)[X]	H-400 × 200 × 8 × 13 (0.90)[L]	H-350 × 200 × 12 × 19 (0.10)[Y]	H-400 × 200 × 8 × 13 (0.90)[L]
2	H-400 × 150 × 12 × 16 (0.15)[X]	H-400 × 200 × 8 × 13 (0.90)[L]	H-450 × 150 × 12 × 16 (0.16)[Y]	H-400 × 200 × 8 × 13 (0.90)[L]
1	H-400 × 250 × 12 × 19 (0.20)[X]	H-400 × 200 × 8 × 13 (0.90)[L]	H-400 × 250 × 12 × 19 (0.19)[Y]	H-400 × 200 × 8 × 13 (0.90)[L]

BRBs in Table 6. Compared to the superior solutions for the braced-frame structures in Table 4, the column sections, C1 and C2, in 1-2 parts are especially small. This is because C_{QUN1} is lower in BRB structures and additional axial forces in columns under the seismic loads in BRB structures are lower.

The results of pushover analysis and response history analysis for the superior solutions of BRB structures are shown in Figures 8-10. The results of pushover analysis mostly satisfy C_{QUN1} = 0.5. The yield inter-story drift ratio of BRBs is 0.1%-0.2%. In the response history analyses, the maximum value of R_{MAX} is 1.4%, and C_{QU1} is 0.46-0.47 for P = 1.0 and 0.43-0.45 for P = 5.0. C_{QU1} values are close to C_{QUN1} because the floor accelerations are controlled by the yielding of BRBs.

Steel volumes of the superior solutions of BRB structures are also shown in Figure 7, where SFS has the smallest and

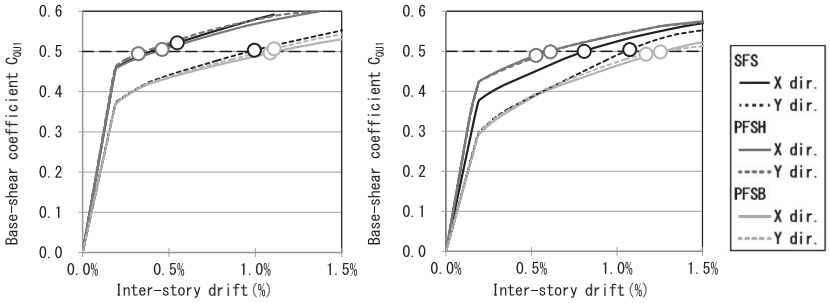

Figure 8. Relationships between base-shear coefficient and inter-story drift ratio of BRB structures

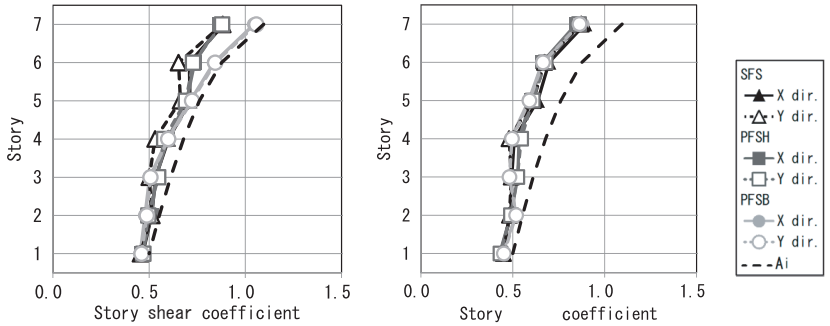

Figure 9. Maximum shear coefficient in BRB structures (Kobe)

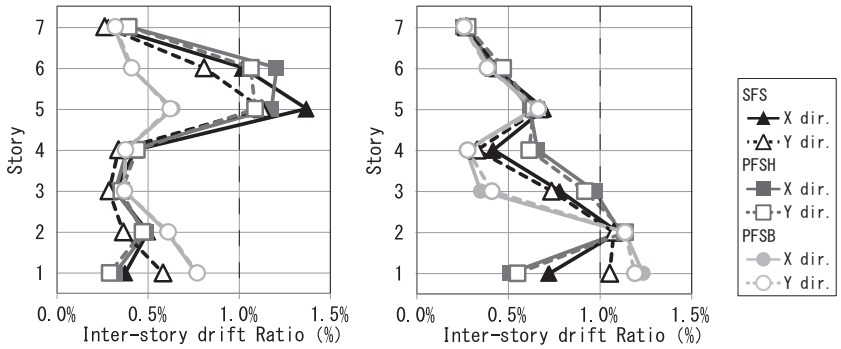

Figure 10. Maximum inter-story drift ratio in BRB structures

PFSH has the largest value among the three types, SFS, PFSH, and PFSB; however, the differences are relatively small. The steel volume excluding BRBs decreases 12%, and the equivalent steel volume of BRBs increases 19%, in the superior solutions with $P = 1.0$ from those with $P = 5.0$. This shows that frames excluding BRBs contribute more to the lateral strength in the case of expensive BRBs. When $P = 5.0$, the steel volume excluding BRBs is 83%-89% that of braced-frame structures. When $P = 1.0$, it is 70%-77%. The effectiveness of BRBs, in terms of their steel volume and structural characteristics, has been quantitatively evaluated based on the results of response history analyses of the BRB and braced-frame structures against L2 earthquakes.

6. Mixed-frame Structures

The structures evaluated in the previous sections have the same building structures (moment frame or braced frame) in the X- and Y-directions in the diagram in Figure 1. In this section, buildings with different structures in the X- and Y-directions with non-uniform column spacing are examined.

6.1 Compositions and grouping

As shown in Figure 11, there is no column on the X2- to X5-axes in the Y2-axis, and the column spacing is 12.8 m between the Y1- and Y3-axes. These long-span beams are called GY2, and beams between Y3 and Y4 are GY3. These beams are pin supported at the ends, and are therefore, secondary beams in PFSH and PFSB. They are assigned as the minimum rolled sections as H-750 × 250 × 12 × 25 and H-400 × 200 × 8 × 13. In SFS, GX1s in the Y4-axis are renamed as GX2, and C2 at the X2- to X5-axes are renamed as C3. The torsional deformation can be controlled by making the lateral frame in the Y1-axis stiffer than the frames in the Y3- and Y4-axes.

6.2 Superior solutions for mixed-frame structure

C_{QUN1} for the X-direction, which is the moment-frame structure, is renamed as C_{QUN1X}, and is assigned as 0.6, while C_{QUN1} for the Y-direction, which is the braced-frame structure, is renamed as C_{QUN1Y}, and is assigned as 1.0. The superior solutions of the mixed-frame structure in SFS, PFSH, and PFSB are obtained and their pushover and response history

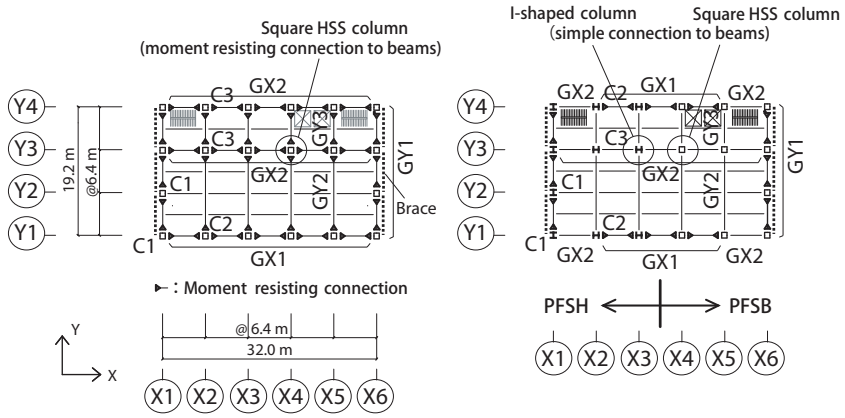

Figure 11. Floor framing plan of mixed-frame structure

analysis results are shown in Figures 12 and 13, respectively. The ultimate lateral strengths mostly satisfy the required strengths of C_{QUN1X} and C_{QUN1Y}. In the response history analyses, the maximum inter-story drift ratio R_{MAX} is approximately 1.5% in the X-direction.

The steel volume of the mixed-frame structure is also shown in Figure 7. The volume is lower, in the order of PFSH (87%), PFSB (96%), and SFS (100%), where the ratios to the volume of SFS are shown in parentheses. The steel volume of SFS is slightly larger than that of PFSB, which is different from the moment-frame structure. This may be because there are some constraints that increase the steel volume for irregular configuration. In particular, the uniform beam height constraint increases beam sections including the 12.8-m long-span Y2 beam, and the strong-column-weak-beam constraint increases column sections.

7. Conclusions

In this paper, superior solutions for a 7-story office building with different lateral frame locations and column shapes were obtained using the MSLS method, and their structural characteristics were investigated. The objective function is the total steel volume to be minimized, and the grouped section sizes are the discrete design variables. The superior solutions satisfy the requirements of the first (allowable stress) and second (ultimate lateral strength) design steps. An algorithm to obtain the solutions with many constraints and discrete variables was demonstrated.

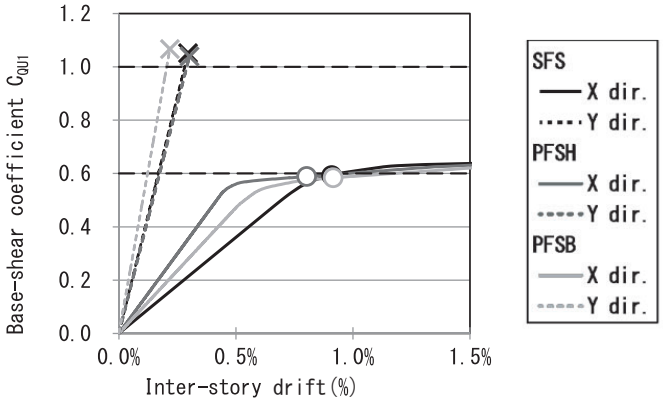

Figure 12. Relationships between base-shear coefficient and inter-story drift ratio of mixed-frame structures

Superior solutions were obtained for three types of structural systems with different lateral frame locations and column shapes, which are (1) SFS with rectangular HSS columns and with lateral frames in all frames, (2) PFS with I-shaped columns and with lateral frames in perimeter frames (PFSH), and (3) PFS with rectangular HSS columns (PFSB). Superior solutions were obtained for three types of building structures: moment frame, braced frame, and mixed frame. For the braced-frame structures, two types of solutions using round HSSs and buckling restrained braces (BRB) were compared. The following findings were obtained:

1 Superior solutions for moment-frame structures were obtained for the required base-shear coefficient of ultimate lateral strength, C_{QUN1}, of 0.3 and 0.6. C_{QUN1} = 0.6 refers to the responses of response history analyses against very rare (L2) earthquake ground motions; however, the maximum inter-story drift ratios are 1.4%-1.5%, which exceed the practically common structural design criteria of 1.0%, that is, none of superior solutions of the three structural systems satisfies the design criteria. The ductility factors are less than 3.0, and the steel volume of the solutions with C_{QUN1} = 0.6 is approximately 1.3 times greater than that with C_{QUN1} = 0.3. The steel volume is lower in the order of PFSH, SFS, and PFSB. Because the seismic performance in these solutions is nearly equivalent in the ultimate lateral strength and maximum ductility factors against L2 earthquakes, PFSH may be more rational in moment-frame structures than SFS, which is a popular system in Japan.
2 The superior solutions for the braced-frame structures were obtained for C_{QUN1} = 0.35 and 1.0. The differences in the steel volume among the structural systems, SFS, PFSH, and PFSB, are relatively smaller than those with moment-frame structures. The steel volume of superior solutions with C_{QUN1} = 1.0 is approximately 1.8 times larger than that with C_{QUN1} = 0.35. The steel volume in PFSH is slightly greater than that of the others. Rectangular HSS columns have advantage over I-shaped sectio, because axial forces are the primary additional structural member forces under the seismic loads.
3 The first natural periods of the superior solutions are 0.92-1.05 seconds for the moment-frame structures and 0.46-0.51 seconds for the braced-frame structures. C_{QUN1} = 0.6

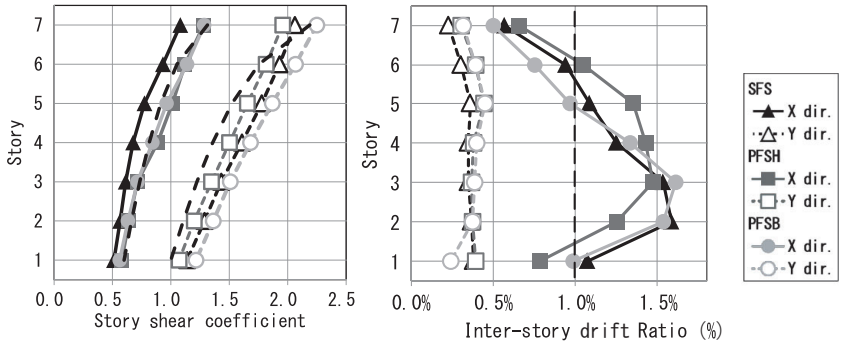

Figure 13. Responses in response history analyses for mixed-frame structures

for the moment-frame structures and $C_{QUN1} = 1.0$ for the braced-frame structures are defined referring to the response in response history analyses against L2 earthquakes and these values are significantly higher than the code required values. Although the 7-story buildings examined can be designed by the ultimate lateral strength calculations or response history analysis, the lateral strength required in these two design approaches is significantly different.

4 The superior solutions of BRB structures were obtained for $C_{QUN1} = 0.5$, replacing the round HSSs with BRBs. The maximum base-shear coefficient C_{MAX1} in response history analyses is 0.43-0.47, and therefore this energy dissipation effect of BRBs has been confirmed. Similar to the braced-frame structures, the steel volume in PFSH is slightly higher than those of other structures. The steel volume excluding BRBs of the superior solutions with the equivalent cost coefficient $P = 1.0$ is 12% smaller than that with $P = 5.0$, and the steel volume of BRB was 19% larger. The steel volume excluding braces in the superior solutions of BRB structure is 70%-90% of that of braced-frame structures with $C_{QUN1} = 1.0$.

5 The steel volume in SFS is larger and the volume in PFSH is smaller in the mixed-frame structures. The steel volume of SFS is larger, which is differrent from the moment-frame structures because constraints on the uniform beam height and strong-column-weak-beam may increase the structural volume under the irregular configuration.

This research examined a 7-story office building with moment-frame, braced-frame (round HSSs and BRBs), and mixed-frame structures. The findings from this limited number of case studies are not sufficient to understand the general structural characteristics of these structures. However, superior solutions were obtained by using the design algorithm independent of engineers' personal experience and skill. Therefore, the discussion and findings comparing these different structural systems have a certain practical merit.

Acknowledgments

This research is partly supported by JSPS KAKENHI Grant Number JP16H0444902, which is greatly appreciated.

Disclosures

The authors do not have any conflicts of interest.

References

1 Mukai H, Nagao T, Hasegawa T, Takahashi K, Seki M, Fukuda K. Comparison between seismic performance of U.S. steel perimeter and Japanese spatial moment resisting frames: Part1–3. Summaries of Technical Papers of Annual Meeting, Architectural Institute of Japan. C-1, Structures III. 1998:903–908. (in Japanese)
2 Kimura Y. Comparison of hysteresis energy and plastic deformation capacity for U.S. and Japan moment resisting frames. Summaries of Technical Papers of Annual Meeting, Architectural Institute of Japan. C-1, Structures III. 2008:761–762. (in Japanese)
3 Taga K, Kohara H. Study on seismic performance evaluation of steel Box column and H-shaped steel column with multi-directional input motion. Summaries of Technical Papers of Annual Meeting, Architectural Institute of Japan. C-1, Structures III. 2012:1035–1036. (in Japanese)
4 Rokugo M, Nagao T. Comparison on seismic of United States and Japan steel moment-frame buildings. Summaries of Technical Papers of Annual Meeting, Architectural Institute of Japan. C-1, Structures III. 2005:943–944. (in Japanese)
5 Mason BF, Kasai K, Ooki Y. Relative performance of Kobe and Northridge WSMF buildings. *Earthquake Spectra*. 1996;**22**:1081–1097.
6 Tagawa H, MacRae G, Lowes L. Probabilistic evaluation of seismic performance of 3-story 3D one- and two-way steel moment-frame structures. *Earthquake Eng Struct Dynam*. 2008;**37**:681–696.
7 Takagi J, Ohsaki M. Comparison of structural characteristics of office buildings composed of space and perimeter frame systems. *Journal of Structural and Construction Engineering (Transactions of AIJ)*. 2015;**715**:1469–1478. (in Japanese)
8 Takagi J, Ohsaki M, Ishikawa S. Ultimate lateral strength and seismic response of steel office buildings composed of space and perimeter frame systems. *Journal of Structural and Construction Engineering (Transactions of AIJ)*. 2016;**728**:1743–1751. (in Japanese)
9 American Society of Civil Engineers (ASCE). Minimum design loads and associated criteria for buildings and other structures (ASCE/SEI 7-16). 2016.
10 National Institute for Land and Infrastructure Management (NILIM), et al. *2015 nendoban-kentikubutsunokouzoukankeigijutsukijun kaisetsusho (Explanation Book of Structural Technology Standard of Buildings 2015)*. 2015. (in Japanese)
11 Bruneau M, Uang CM, Sabelli R. *Ductile Design of Steel Structures*, Second Edition. New York, NY: Mc-Graw Hill Education; 2011.
12 The Building Center of Japan. *The Building Standard Law of Japan on CD ROM*. Tokyo, Japan: The Building Center of Japan (BCJ); 2016.
13 Kubo M, Pedroso JP. *Metaheuristics: A Programming Guide*. Japan: Kyoritsu Shuppan Co., Ltd.; 2009. (in Japanese)
14 Midas GEN Ver. 800. *MIDAS Information Technology*. Gyeonggi-do, South Korea: MIDAS Information Technology Co., Ltd.; 2014.
15 Nippon Steel & Sumitomo Metal Corporation. *Kensetsuyou-Shizai Handbook*. 2012. (in Japanese)
16 SNAP Ver.6.0.1.3. Kozo System, Inc. 2016.
17 Shibata M, Nakamura T, Wakabayashi M. Mathematical expression of hysteretic behavior of braces, Part 1 derivation of hysteresis functions. *Transactions of the Architectural Institute of Japan*. 1982;**316**:18–23. (in Japanese)
18 Shibata M, Nakamura T, Wakabayashi M. Mathematical expression of hysteretic behavior of braces, Part 2 application to dynamic response analysis. *Transactions of the Architectural Institute of Japan*. 1982;**320**:29–35. (in Japanese)
19 Taniguchi H, et al. Study on restoring force characteristics of steel frames in building of nuclear power stations Part 6 simulation analysis. Summaries of

Technical Papers of Annual Meeting, Architectural Institute of Japan. Structures II, 1990:1541–1542. (in Japanese)
20 JFE Civil Engineering & Construction Corp. *Tube-in-Tube Buckling-Restrained Braces Hyojunbuzaihyo*. 2016. (in Japanese)
21 The Building Center of Japan. Tube-in-Tube Buckling-Restrained ST0010-05. 2016. (in Japanese)
22 Architectural Institute of Japan. *AIJ Design Standard for Steel Structures—Based on Allowable Stress Concept*—(2005 Edition). 2017.

How to cite this article: Takagi J, Obana R, Ohsaki M. Superior design solutions of section sizes in steel buildings for different lateral frame systems and column shapes. *Jpn Archit Rev*. 2020;3:445–458. https://doi.org/10.1002/2475-8876.12156

Appendix 1

Steel deck slabs are used for the floor structure in the building examined. The slabs are extended 400 mm from the perimeter axes shown in Figure 1; therefore, the floor area is 656 m^2. The floor weights per unit area are 7.8 and 6.8 kN/m^2 for the frame design and seismic design, respectively. The average exterior weight per unit elevation area is assumed as 2.0 kN/m^2. Therefore, the total weights per floor area are 9.0 and 8.0 kN/m^2 for the frame design and seismic design, respectively. The weights are input in the 3D frame models as concentrated loads at the nodes connecting beams and columns, and nodes at every 3.2 m in the beams. The roof weight is typically heavier than office floors but assumed to be the same for simplicity.

Appendix 2

Modeling Assumptions for Elastic Analyses

1 Floor diaphragm condition is adopted.
2 Columns are divided into two elements at the center of floors. Beams are divided every 3.2 m.
3 The bottoms of first floor columns are supported and rotationally fixed. The braces are pin connected.
4 The composite effect between steel beams and concrete slabs is disregarded.
5 The fillet part of I-shaped sections is disregarded.
6 The rigid zone in the beam-to-column connections is disregarded.
7 Shear deformations in members are disregarded.

Modeling Assumptions for Pushover Analyses

1 Simple-step pushover analyses are conducted with the increments of lateral loads. (No iterative calculation is performed in each load step.)
2 The vertical distribution factor, A_i, is assumed for the seismic loads. The base-shear coefficient of load increment in one step in the pushover analyses is approximately 0.002.
3 Lumped rotational inelastic springs are placed at the ends of beams and columns. The springs are bilinear with sufficiently stiff initial stiffness and 1/100 of the flexural stiffness of the element for the post-yielding stiffness.
4 The yielding moment of the lumped rotational springs is defined as the plastic moment, $M_p = 1.1FZ_p$, where F is the design standard strength (nearly nominal yield strength) of the steel and Z_p is the plastic section modulus.
5 The tensile yielding strength N_Y and compressive buckling strength N_C of the braces are defined as $1.1FA$ and $1.1f_{CS}A$, respectively, where A is the cross-sectional area and f_{CS} is the temporary allowable compressive stress.
6 The P-Delta effect is not taken into account.

Appendix 3

The constraints of MSLS are summarized below. The symbols are defined in Table 2.

No.	Lateral System	Constraints	
1	All	$\sigma \leqq \sigma_a$ Allowable stress constraints	[a]
2		Width-thickness constraints for beams and columns with A or B rank (eg, $D_c/t_c \leqq 31.4$)	[b]
3		Width-thickness constraint for brace round HSSs with A or B rank (eg, $D_p/t_p \leqq 60$)	[c]
4		$t_f/t_w \geqq 1.3$ for beams	[d]
5		Strong-column-weak-beam constraint, $\Sigma M_{pc} \geqq \Sigma 1.5M_{pb}$	[e]
6		Beam sagging constraint, $\delta < L/300$	
7		Inter-story drift constraint under seismic design load, $R \leqq 0.5\%$	
8		Ultimate lateral strength constraint, $C_{QUN1} \leqq C_{QU1}$	[f]
9	SFS	Uniform beam height in a floor	[g]
10	SFS PFSB	Uniform column width	
11	PFSH	Uniform column height (non-uniform flange width)	

[a]The allowable stress is defined in the "AIJ Design Standard for Steel Structures".[22] Beams are assumed to be laterally supported.
[b]The width-thickness ratios for members with A or B rank for SN490 steel shall be satisfied.
[c]The slenderness ratios of the round HSS braces shall be less than 49.3. The ranks of round HSS braces are A or B. Referring to the standard round HSSs, $D_p/t_p \leqq 60$ is assumed, where D_p is the diameter and t_p is the plate thickness of the round HSSs.
[d]Optimized I-shaped sections often have relatively large height with thin flange thickness. In order to avoid the sections significantly different from standard section sizes, the constraint of $t_f/t_w \geqq 1.3$ is introduced for the beams. This constraint is not applicable for the columns, where the uniform height is assumed and built-up sections may be used.
[e]The sum of the plastic moment of columns ΣM_{pc} shall be greater than 1.5 times the sum of the plastic moment of beams ΣM_{pb} in each floor.[22] This is required by the Japanese code for cold-form rectangular HSS columns but not for I-shaped columns; however, this is applied for all columns in this research.
[f]The base-shear coefficient of ultimate lateral strength C_{QU1} shall be greater than the required base-shear coefficient C_{QUN1}.
[g]The beam heights in a floor shall be uniform in SFS, as in Japanese practice, thus simplifying the beam-to-column connection details with straight splices between the beam flanges and diaphragm plates in columns.